Twentieth-Century Climate Change over Africa: Seasonal Hydroclimate Trends and Sahara Desert Expansion

Natalie Thomas

A scholarly paper in partial fulfillment of the requirements for the degree of

Master of Science

December 2018

Department of Atmospheric and Oceanic Science, University of Maryland
College Park, Maryland

Advisor: Dr. Sumant Nigam

Table of Contents

Abstract

Twentieth-century trends in seasonal temperature and precipitation over the African continent are analyzed from observational datasets. Given the agricultural economy of the continent, a seasonal perspective is adopted as it is more pertinent than an annual-average one, which can mask offsetting but agriculturally sensitive seasonal hydroclimate variations. Examination of linear trends in seasonal surface air temperature (SAT) shows that heat stress has increased in several regions, including Sudan and northern Africa where the largest SAT trends occur in the warm season. Broadly speaking, the northern continent has warmed more than the southern one in all seasons. Precipitation trends are varied but notable declining trends are found in the countries along the Gulf of Guinea, especially in the source region of the Niger River in West Africa, and in the Congo River basin. Rainfall over the African Great Lakes—one of the largest freshwater repositories—has, however, increased. It is shown that the Sahara Desert has expanded significantly over the twentieth century, by 11%–18% depending on the season, and by 10% when defined using annual rainfall. The expansion rate is sensitively dependent on the analysis period in view of the multidecadal periods of desert expansion (including from the drying of the Sahel in the 1950s–80s) and contraction in the 1902–2013 record, and the stability of the rain gauge network. The desert expanded southward in summer, reflecting retreat of the northern edge of the Sahel rainfall belt, and to the north in winter, indicating potential impact of the widening of the tropics. Specific mechanisms for the expansion are investigated.

Acknowledgements

I would like to thank my adviser, Dr. Sumant Nigam, for the excellent guidance and encouragement on this project and throughout my time at the University of Maryland. Thank you also to Dr. Alfredo Ruiz-Barradas for help with data sets and analysis techniques.

List of Tables

List of Figures

Chapter 1. Introduction

1.1 Background

Climate change has footprints across the planet; however, certain regions are disproportionately affected. Africa is less responsible for the occurrence of anthropogenic climate change than any other continent (Fields 2005) but more vulnerable to its effects on account of its high population, low adaptive capacity, and multiple converging stressors (Busby et al. 2014; Fields 2005; Niang et al. 2014). Africa is furthermore an interesting case study for climate change due to its unique climatological features. It is the only continent that has almost equal parts in the Southern and Northern Hemispheres (Collins 2011) and thus is home to a wide variety of climate zones. It consists of the Sahara Desert and Sahel in northern Africa, the Namib-Kalahari Desert in southern Africa, tropical rain forest in equatorial Africa, and grasslands and savanna in between. The prevalence of land surface effects, internal climate variability, and sensitivity to global sea surface temperatures make the continent climatically complicated (Hulme et al. 2001).

Several studies have investigated the trends in precipitation and surface air temperature over the continent. Precipitation variability occurs on a range of climate time scales; low-frequency variability, characteristic of West Africa and the Sahel, is associated with multidecadal changes in sea surface temperature (SST) and atmospheric circulation (Nicholson 2001; Nigam and Ruiz-Barradas 2016; Zhang and Delworth 2006) whereas higher-frequency variability, seen in eastern and southern Africa (Nicholson and Kim 1997; Schreck and Semazzi 2004) is connected to El Nino-Southern Oscillation

(ENSO) and other subdecadal processes (Hulme et al. 2001; Nicholson 2001; Omondi et al. 2013).

Precipitation trends have been particularly well studied over the Sahel region. The drying trends have been related to land surface processes, including amplification of meteorological drought from biophysical (Charney 1975) and surface hydrologic feedbacks (Nicholson 2000). Regional and global patterns of SST anomalies have also been implicated (Folland et al. 1986; Giannini et al. 2003) as have sulfate aerosols in the Northern Hemisphere through their effect on Atlantic SSTs (Biasutti and Giannini 2006). The 1980s Sahel drought – the most intense episode of the twentieth century – has been attributed to the circulation change associated with Indian Ocean warming (Hagos and Cook 2008), and the drought recovery linked to higher levels of greenhouse gases in the atmosphere (Dong and Sutton 2015). Sahel rainfall has also been linked to Atlantic multidecadal oscillation (AMO) variability (Knight et al. 2006; Martin and Thorncroft 2014; Mohino et al. 2011; Nigam and Ruiz-Barradas 2016; Nigam et al. 2011; Zhang and Delworth 2006), with the cold AMO phase coincident with extended droughts over the Sahel.

Causes of surface temperature variability are less well established (Collins 2011), although an amplified warming signal has been detected over the Sahara Desert in recent decades (Cook and Vizy 2015; Vizy and Cook 2017; Zhou 2016).

The importance of agriculture in the African economies warrants a seasonally resolved analysis of hydroclimate variability and change over the African continent. The seasonality of trends in temperature and precipitation over Africa has been briefly examined in earlier studies. Temperature trends over the continent as a whole were

found to be greater in summer and fall than in winter and spring (Collins 2011; Hulme et al. 2001), with significant winter warming in northern tropical Africa and significant summer warming across the continent, and specifically the Sahara (Collins 2011). Documented precipitation trends, other than over the Sahel, include the decreasing spring rainfall trend over East Africa (Maidment et al. 2015; Rowell et al. 2015; Williams and Funk 2011) and continental-scale seasonal precipitation trends (Hoerling et al. 2006); the latter have been plotted but not extensively discussed. The need to analyzing seasonal rainfall in tropical regions has been noted (Feng et al. 2013).

Global climate change often leads to the wet regions getting wetter and the dry ones drier (Chou et al. 2013), suggesting adverse impacts on deserts. The impact on the Sahara is of great importance for the proximal countries in northern Africa as well as for remote regions through the influence of Saharan dust on SSTs and Atlantic hurricane activity (Evan et al. 2016). Previous studies have estimated the size of the annual-mean Sahara Desert (Tucker and Nicholson 1999; Tucker et al. 1991) but only over the recent satellite-era periods ranging from 10 to 17 years. The century-long seasonal trends in the expanse and extent of the Sahara Desert, whose structure and mechanisms concern this study, have hitherto remained undocumented. A seasonally stratified perspective is at some variance with the classical notion of the desert (based on an annual-mean view) but is nonetheless pursued in the interest of agriculture and water resource planning. It is, of course, complemented by analyses of the annual-mean hydroclimate trends, yielding twentieth century expansion rates for the conventionally defined Sahara Desert.

1.2 Objectives of this study

The present study expands on previous work by examining the regional structure of the century-long seasonal trends in temperature and precipitation over the African continent, with the Saharan expanse being one of the foci. Characterization of the trends is a necessary first step before investigation of the underlying mechanisms; a follow-on study targeting the mechanisms is planned. The datasets and analysis methods are described in Chapter 2. Chapter 3 describes the seasonal climatology of near surface air temperature (SAT) and precipitation over the African continent , the century-long seasonal hydroclimate trends, the expansion of the Sahara Desert over the twentieth century and the winter and summer expansion mechanisms. Concluding remarks, including the influence of multidecadal SST variability on the Sahara Desert's twentieth-century expansion rate, and plans for future work follow in Chapter 4.

Chapter 2. Data and Methods

This study focuses on centennial trends rather than multidecadal variability (a more common analysis focus) of African hydroclimate. Linear trends in temperature and precipitation are computed from least squares fitting using seasonally averaged data. To avoid confusion given Africa's expansive footprints in both hemispheres, seasons are referred using their boreal definition: winter is the average of December, January, and February (DJF), and so on.

2.1 Observational Data Sets

Three independent analysis of the observed SAT are used in this study. The CRU-TS 4.00 monthly analysis from the Climate Research Unit of the University of East Anglia (Harris et al. 2014) is available on a 0.5° continental grid for the January 1902-December 2014 period from http://www.crudata.uea.ac.uk/cru/data/hrg/cru_ts_4.00/. Berkeley Earth's monthly analysis of surface temperature anomalies relative to the 1951-80 climatology (Rohde et al. 2013) is available on a 1.0° grid for the period January 1850-December 2015; it is downloadable from http://berkeleyearth.org/data. Finally, the NASA Goddard Institute for Space Studies (GISS) analysis of SAT anomalies relative to the 1951–80 baseline (Hansen et al. 2010) is available on a 2.0° land-ocean grid for the January 1880-September 2015 period from http://www.esrl.noaa.gov/psd/data/gridded/data.gistemp.html. The datasets are converted to a common 0.5° resolution using bilinear spatial interpolation.

The Global Precipitation Climatology Centre (GPCC) provides a monthly analysis of precipitation from quality-controlled station gauge data (Becker et al. 2013). GPCC's full data reanalysis version 7 data, available on a 0.5° continental grid for the

January 1901-December 2013 period, are used here (see http://www.esrl.noaa.gov/psd/data/gridded/data.gpcc.html#detail). From the several available analyses of continental precipitation (including CRU-TS), the GPCC analysis was chosen because of the larger number of stations used in the development of this gridded product, especially relative to CRU-TS and the Global Historical Climatology Network (GHCN) – see the NCAR Climate Data Guide. The monthly precipitation database informing the GPCC analysis is, perhaps, the largest among the competing analyses (Schneider et al. 2014), prompting its use in constraining NASA's Tropical Rainfall Measuring Mission (TRMM) precipitation. Sahel rainfall is defined as the area-averaged rainfall within 20°W-40°E and 10°N-20°N, following Held et al (Held et al. 2006).

The NCEP-NCAR reanalysis (Kalnay et al. 1996) is used for calculating the core latitude of the subtropical tropospheric jet in northern winter, following the method of Archer and Caldeira (2008) with integration over the latitude band 15°N-45°N.

Several climate indices are used in this chapter. The Atlantic multidecadal oscillation (Enfield et al. 2001; Kavvada et al. 2013) index was computed as the linearly detrended seasonal SST anomaly over the North Atlantic (0°-60°N, 5°-75°W), following Enfield et al. (2001); SST from the HadISSTv1.1 analysis (Rayner et al. 2003) was used. An additional marker of AMO variability was the principal component extracted from an extended empirical orthogonal function (Weare and Nasstrom 1982) analysis of HadISSTv1.1 SST data (Guan and Nigam 2009). The Pacific decadal oscillation (PDO) index was obtained from http://jisao.washington.edu/data/pdo/ where it is defined as the

leading principal component of monthly SST anomalies in the North Pacific (poleward of 20°N) (Zhang et al. 1997).

Streamflow data for the Niger River were obtained from NCAR's monthly flow rate archive (https://rda.ucar.edu/datasets/ds552.1) (Dai and Trenberth 2003). Station 9142 (Koulikoro; 12.887°N, 7.54°W) was used as it has the longest record among stations in the source region of the Niger River. The record extends from January 1902 to December 1990.

2.2 Desert Expansion

Two methods are used to quantify desert expansion during the 1902-2013 period. In both methods, a precipitation threshold is chosen to define the desert boundary; two threshold values – 100 mm/yr (or 0.274 mm/day) and 150 mm/year (or 0.411 mm/day) – based on previous definitions of the annual-mean Sahara boundary (Breman and Dewit 1983; Tucker and Nicholson 1999) are used. Two thresholds were considered so that sensitivity of the desert-area trend to the desert definition can be assessed. Desert area is computed by taking an area sum after weighting each grid-cell area by the cosine of its latitude; the Grid Analysis and Display System (GrADS) function 'asum' was used. In the first method, referred to as the area-trend method, the desert area is computed each year in each of the four seasons and annually, with average rainfall less than 0.274mmday21 (0.411mmday21) defining deserts. The 1902–2013 linear trend in the computed area characterizes desert expansion/contraction over the twentieth century.

In the second method, referred to as the endpoint method, the precipitation climatology (P_{clim}) and the linear trend in precipitation (Pt_{rend}) over the 112-yr record are first computed at each grid point, seasonally and annually. These are used to create two

maps, showing precipitation at the end (from the plus sign in the following expression) and at the beginning (from the minus sign) of the record:

$$P = P_{clim} \pm (P_{trend}) \times 56 years$$

The desert extent is then mapped in these synthetic 1902 and 2013 precipitation distributions at the endpoints of the record based on the chosen threshold, with the difference yielding desert expansion over the time period.

In both methods, the desert area computation is restricted to North Africa (northward of 58°N) to preclude inclusion of the Namib–Kalahari Desert, and to the west of 43°E to avoid inclusion of the Horn of Africa.

Each method has its advantages: The area-trend method is conceptually simple, but it does not reveal the desert advance and retreat regions. The endpoint method is slightly more complex but it easily outlines the desert advance/retreat regions. Both methods should yield similar results except, perhaps, when the analysis period is comparable to the embedded variability time scales—a condition met with the AMO, especially when it is influential on regional hydroclimate. The aliasing of multidecadal variability into linear trends would be inevitable in this case but with the two methods having different exposure to aliasing from the inverted order of the area-computation and linear-trend operations.

The seasonal northern edge of the Sahara Desert was computed each year as follows: For each desert longitude (20°W–35°E), the nearest latitude north of 20°N where the seasonal precipitation threshold was met was determined. The latitudes were then averaged to obtain the northern edge of the Sahara Desert.

2.3 Statistical significance

Statistical significance of individual linear trends at the 95% confidence level was assessed using the so-called AdjSE+AdjDF approach of Santer et al. (2000). This method employs an effective sample size based on the lag-1 autocorrelation coefficient of the regression residuals. The statistical significance of correlation coefficients was calculated using the method outlined in Ebisuzaki (1997), which is useful for time series with high serial correlation. Significance of the correlation coefficients is noted in the text.

Chapter 3. Results

3.1 Seasonal Climatology

The seasonal cycle of rainfall over the African continent is shown in Figure 1. Rainfall is larger, not surprisingly, in the summer hemisphere: over tropical West Africa, the Sahel, and Ethiopia in boreal summer (JJA) and over the Congo and Zambezi basins in austral summer (DJF). The similarity of the March–May and September–November rainfall distributions—with equatorial Africa, especially the Congo basin, being the rainfall focus—reflects the similar insolation distribution over the continent at these times from the Sun being overhead twice at the equator each year, during the vernal (late March) and autumnal (late September) equinox. The Sahara Desert is, however, drier in spring than it is in fall, and the Namib–Kalahari Desert likewise is drier in its spring than fall. The strong latitudinal gradient in precipitation at the southern boundary of the Sahara is a notable feature in all seasons, with the movement of this gradient over time having implications for regional agricultural productivity.

The desert boundary, based on seasonally averaged rainfall threshold of 0.274 mm day^{-1} (or 25 mm $season^{-1}$), is shown in thick black contours in Figure 1. The Sahara expanse is largest in boreal winter and smallest in boreal fall (see Table 1); the larger threshold (0.411 mm day^{-1} or 37.5 mm $season^{-1}$) yields the smallest expanse in summer; both analysis methods return the same seasons for maximum and minimum expanse (cf. Table 1). In winter, the dry region extends from ~10° to 30°N, but in summer the Sahel rainfall pushes the Sahara's southern edge closer to 20°N. Likewise, the Namib–Kalahari Desert in Southern Hemisphere Africa is most expansive in austral winter, consistent with the notion of the desert location under the descending branch of the meridionally

overturning Hadley circulation; the Hadley descent is most intense in each hemisphere's winter (Nigam and Chan 2009).

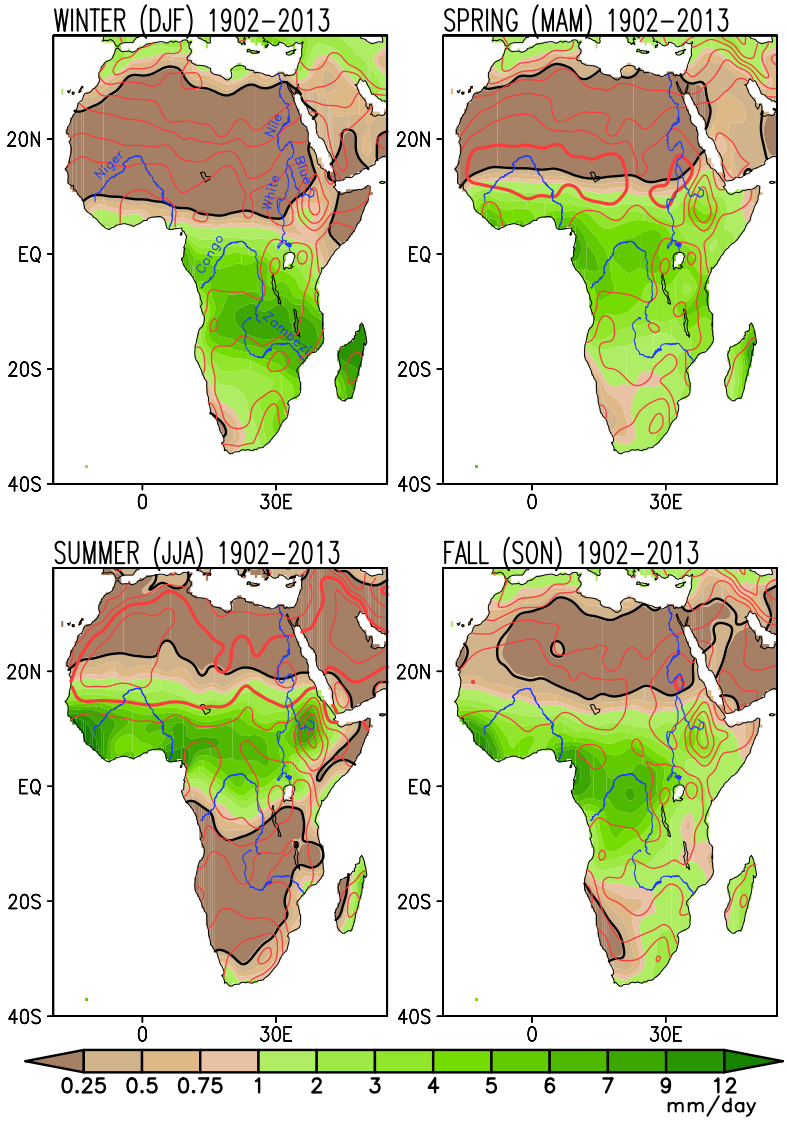

Figure 1. Seasonally averaged precipitation (brown–green shading; mm day-1) and surface air temperature (SAT; red contours; °C) for the period 1902–2013. Precipitation is from GPCC and SAT from the CRU TS4.00 dataset. Contour interval for SAT is 3.0°C. Fields are shown after nine applications of the 9-point smoother (smth9) in GrADS. Thick red contours indicate the 30°C isotherm, while thick black ones mark the 0.274mm day-1 precipitation isoline.

The seasonal distribution of climatological SAT is also shown in Figure 1, using red contours. The warmest temperatures are found in boreal summer when SAT exceeds 33°C over western Saharan Africa. The coldest temperatures occur northward of the

Atlas Mountains in Algeria and Morocco in boreal winter. A local minimum in SAT exists over Ethiopia in all four seasons due to the high elevation of the Ethiopian Highlands. The spring and fall distributions exhibit less similarity in SAT than in rainfall, especially over sub-Saharan Africa where SAT is notably higher in boreal spring, likely because of the preceding dry season (winter) and depleted soil moisture stores, which would preclude latent disposition of increased spring insolation.

3.2 Centennial Trends in Surface air Temperature and Precipitation

The 1902-2014 SAT trend, obtained from the average trend in three independent analyses (CRU TS4.00, Berkeley Earth, and NASA GISS) of SAT observations, is shown in Figure 2. Notable features include the following:

- Larger trends over Northern Hemisphere Africa in all seasons.
- A regional maximum over Sudan, particularly in spring when SAT trends are larger than 1.5°C century^{-1}; interestingly, this is the Nile River basin.
- A pronounced seasonality in trends over North Africa, near Algeria and Tunisia. Trends here range from 0.8°C century^{-1} in winter to 2.0°C century^{-1} in summer.
- A comparatively muted seasonality in trends over Southern Hemisphere Africa except for Angola, Namibia, and Botswana where austral winter (JJA) warming is stronger than in other seasons.
- The similarity in boreal winter and fall SAT trends over much of the continent.

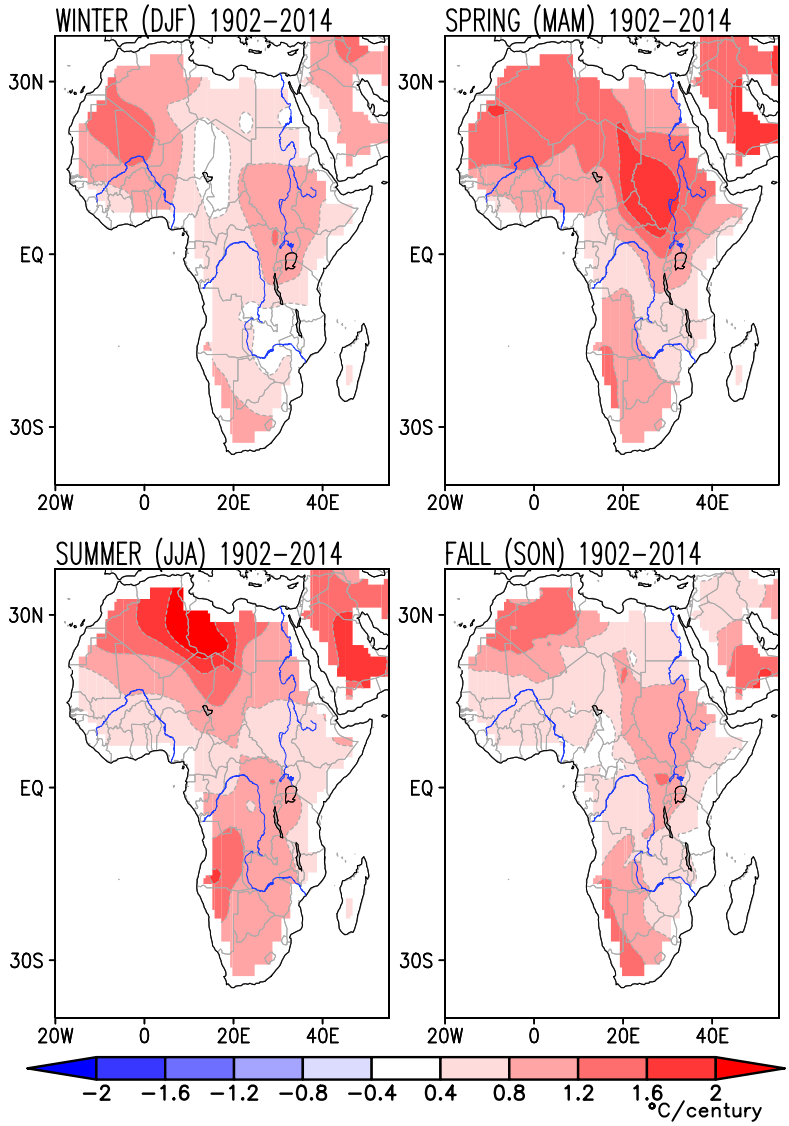

Figure 2. Linear trends in near-surface air temperature over the African continent during 1902–2014. Average of the trends in three independent SAT analyses—CRU TS4.00, Berkeley Earth, and NASA GISS—is shown after each was interpolated to 0.5° resolution. Contour and shading are at 0.4°C century-1 interval.

The seasonality of SAT trends can potentially modulate the amplitude of the seasonal cycle of SAT in the recent period. An increasing amplitude can worsen heat stress, as over central-southern Sudan (to the west of the White Nile) where twentieth-century SAT trends are large, especially in spring when the SAT peaks climatologically as well (cf. Figure 1), leading to hotter springs and increased heat stress. Likewise, over

northern Africa, including Algeria, Tunisia, and Libya, SAT trends are largest in summer, the season of greatest climatological SAT. In both these regions, the SAT trends amplify the seasonal cycle of regional SAT, intensifying heat extremes.

The linear trend in seasonal precipitation over the twentieth century (1902–2013) is shown in Figure 3 against the backdrop of the climatological dry regions (brown hatching). The centennial trends show interesting variations, corroborating the importance of seasonal analysis. For example, over Kenya and Tanzania, declining rainfall trends are present in boreal spring whereas increasing ones are present in fall and winter, each with socioeconomic implications. An annual-mean perspective, where offsetting seasonal trends average out, is not sufficient to understand the impact of climate change on a continent where the seasonal rhythm of rainfall is the pace maker.

The rainfall decline is notably intense, with no seasonal offsets, over tropical West Africa. The decline is broadly focused on the source region of the Niger River, extending across several Gulf of Guinea rim countries (Senegal, Gambia, Guinea-Bissau, Guinea, Sierra Leone, Liberia, and Cote d'Ivoire). The rainfall decline exceeds 1.0 mm day^{-1} $century^{-1}$ here (i.e., a 10%–25% decline in seasonal rainfall over the course of the twentieth century). The boreal spring decline is most impressive, percent-wise, and must lead to an increasing delay in the build-up of Niger streamflow after the winter season.

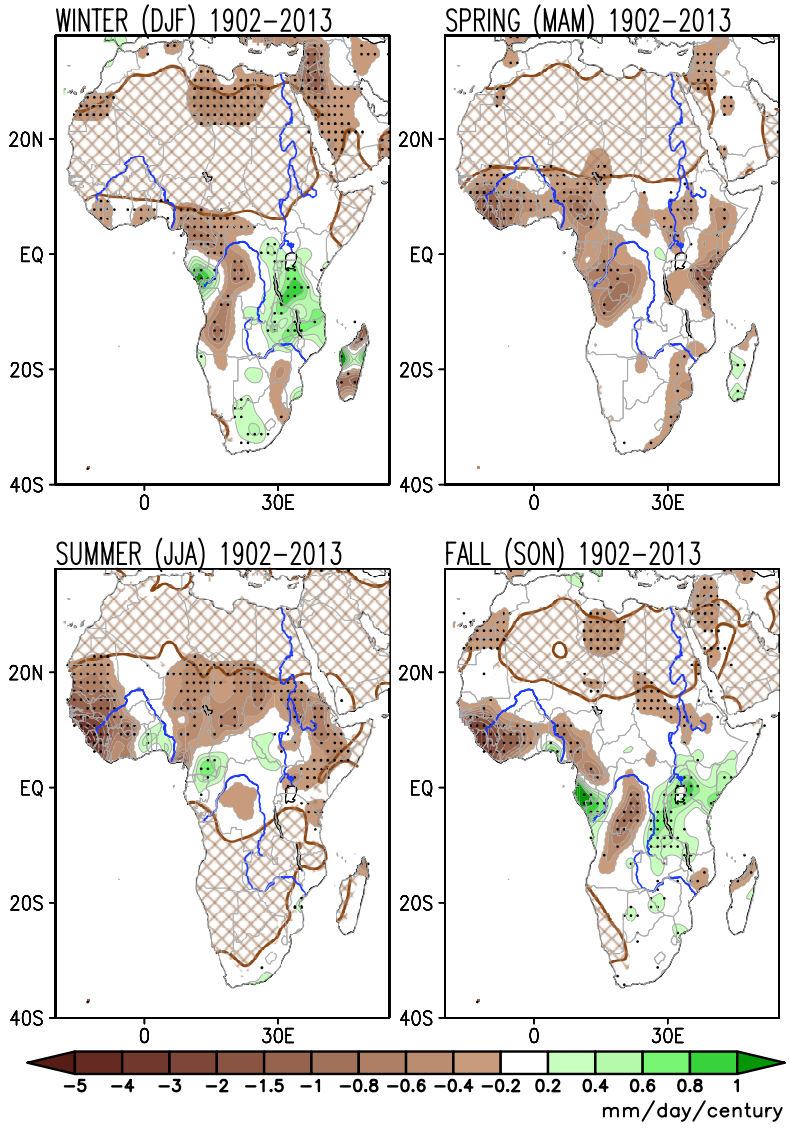

Figure 3. Linear trends in seasonal precipitation over the African continent during 1902–2013, from the 0.5° resolution GPCC dataset (mmday-1 century-1). Thick solid brown contours mark the 0.274mm day-1 climatological precipitation isoline, and brown hatching indicates regions where climatological precipitation is below 0.274mm day-1 (or 100mmyr-1)—a precipitation threshold used for defining the Sahara Desert. Trends significant at the 95%confidence level are denoted with black dots.

Figure 4 shows the monthly streamflow climatology (red line) and trends (black bars) over the 1907–90 period at a monitoring station in the Niger River source region. Climatological streamflow is weakest in spring even though regional precipitation is not a minimum in this season (Figure 1) in part because spring rainfall is effectively used in

recharging soil moisture after the dry season (boreal winter). Even otherwise, a 1–2-month lag of streamflow vis-à-vis regional precipitation is not uncommon because of the aggregation and drainage delays generated in large watersheds, and the temporal phasing of other surface water losses (e.g., evapotranspiration). The streamflow peaks in September, following the wet season (June–August; Figure 1), again with some delay. It is thus not surprising that the streamflow trend is most negative in fall— that is, following the season of most negative precipitation trends (summer, Figure 3). The decline in Niger River's source region streamflow in September is very steep: A 15m^3 s^{-1} yearly decrease, or a 1500m^3 s^{-1} centennial decrease where the climatological flow is ~5000m^3 s^{-1}, represents a 30% reduction over the twentieth century.

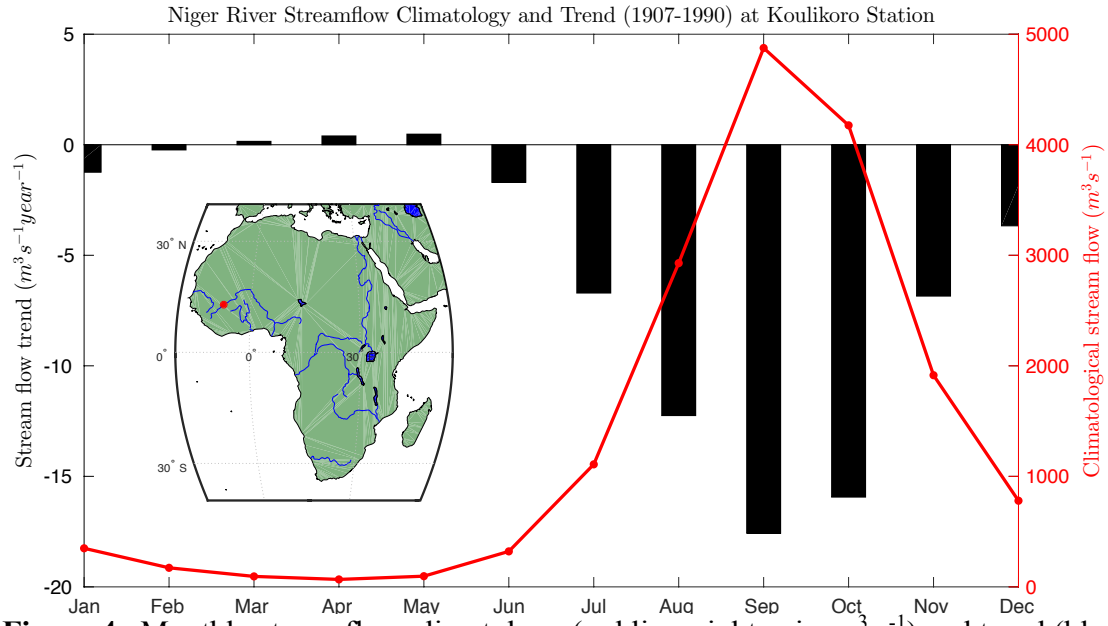

Figure 4. Monthly streamflow climatology (red line; right axis; m^3 s^{-1}) and trend (black bars; left axis; m^3 s^{-1} yr^{-1}) for the 1907–90 period at the Koulikoro monitoring station (12.8878N, 7.548W) in western Mali. The station location in the source region of the Niger River is shown using the red dot in the inset map.

Another region showing rainfall decline in all seasons is the Congo River basin, especially the part encompassing Angola and the Democratic Republic of the Congo.

Rainfall decline here is impressive in the shoulder seasons (spring and fall), with trends exceeding 0.6 mm day^{-1} $century^{-1}$ where seasonal rainfall is 6.0 mm day^{-1}. The thick brown lines in Figure 3 mark the climatological dry zones, facilitating a visual assessment of desert expansion–contraction over the twentieth century (the focus of section 3.5).

The African Great Lakes region, especially Victoria and Tanganyika, is one of the few regions on the continent exhibiting increasing twentieth-century rainfall, mostly in austral spring and summer. This is interesting because of the proximity of this region to the source of the Nile River, and implications for streamflow in the downriver region.

The advantages of a seasonal rather than an annual mean perspective in the context of centennial change in regional hydroclimate over Africa can be gleaned from a comparison of Figures 2 and 3 with their annual-mean counterparts. Figure 5 displays the linear trends in annual SAT and precipitation over Africa. While annual-mean trends clarify the regions of greatest warming and drying on the continent, they can mask notable subannual (i.e., interseasonal) variations in trends that can modulate the regional seasonal cycle: For example, Figure 5 shows maximum annual SAT trends over Sudan and northern Africa but the amplification of the seasonal cycle and related intensification of heat distress is only ascertainable from the structure of seasonal trends. The annual perspective can sometimes be misleading as well, as in the case of precipitation trends over Kenya/Tanzania, which are notable in most seasons but offsetting, leading to an annual-mean trend of close to zero. The impact on agriculture, however, need not be negligible as it is sensitive primarily to the growing seasons' trends.

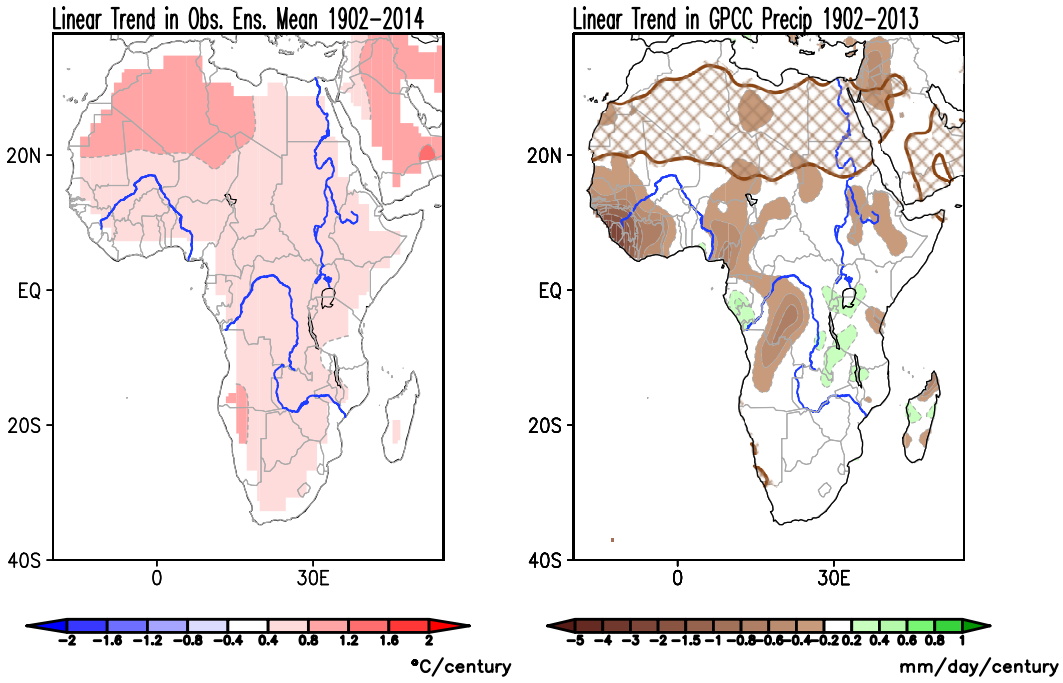

Figure 5. Linear trend in annual-mean (left) SAT (°C century^{-1}) and (right) precipitation (mm day^{-1} century^{-1}) over the 1902–2014 period (1902–2013 for precipitation). The SAT trend is the average of the trends in three independent analyses of SAT observations (as in Figure 2), while the precipitation one is based on the GPCC analysis (as in Figure 3). Thick solid brown contours mark the 100mm yr^{-1} climatological annual-mean precipitation isoline, and brown hatching indicates regions where climatological annual-mean precipitation is less than 100mm yr^{-1}. Both datasets are at 0.5° resolution. Contour and shading interval is 0.4°C century^{-1} for SAT and as indicated by the brown–green color bar for precipitation.

3.3 Change in the expanse of the Sahara Desert over the twentieth century

The overlay of twentieth-century precipitation trends on the climatological dry zones in Figure 3 suggests that the Sahara Desert has expanded both equatorward and northward. The Sahara's extent has been investigated using vegetation-zone boundaries as markers of desert expanse and its interannual variation (Tucker and Nicholson 1999; Tucker et al. 1991). Although interesting because of the implicit seasonal context, these studies analyzed short records such as the recent 10–17-yr-long satellite-era ones. Unfortunately, desert trends over such periods reveal little about the secular changes in

the Sahara because of the potential aliasing of decadal to multidecadal variability into short period trends.

Here, we use the precipitation rate to demarcate the desert region. The use of precipitation rather than vegetation allows analysis of a longer record notwithstanding the spatiotemporal sparseness of the precipitation record in the early twentieth century. A direct relationship between precipitation and the vegetation index found in previous studies (Tucker and Nicholson 1999; Tucker et al. 1991) supports such a strategy. In Figure 3, a 100mm yr^{-1} (or 0.274mm day^{-1}; one of the two thresholds discussed in Chapter 2) precipitation isoline demarcates the deserts, seasonally (and in Figure 5, annually). A light brown hatching of the regions where climatological precipitation is less than this value marks the desert expanse, which is monitored using the two methods discussed in section Chapter 2

The twentieth-century change in the Sahara Desert's seasonal and annual extent is displayed in Figures 6 and 7; the change is estimated using the endpoint method. Brown shading, which represents the desert's advance over the century, shows significant northward creep in boreal winter albeit not uniformly across longitudes; hefty footprints over Libya and Algeria in the central sector, and over the western Sahara and Mauritania to the west, characterize the northward expansion in winter. The desert has encroached equatorward as well in winter, with notable intrusions in Nigeria, Cameroon, and the Central African Republic.

The centennial change in the Sahara's summer extent is through the equatorward advance of its southern boundary which is climatologically located at ~20°N because of robust summer rainfall in the northern tropics including the Sahel (0°–20°N; cf. Figure

1). Much as with the winter desert advance at the northern boundary, the southern advance is sectorally focused, with intrusions in Mauritania to the west and Niger and Chad in the central sector. The countries most impacted by the Sahara Desert's seasonal and annual-mean advance are listed in Tables 1 and 2.

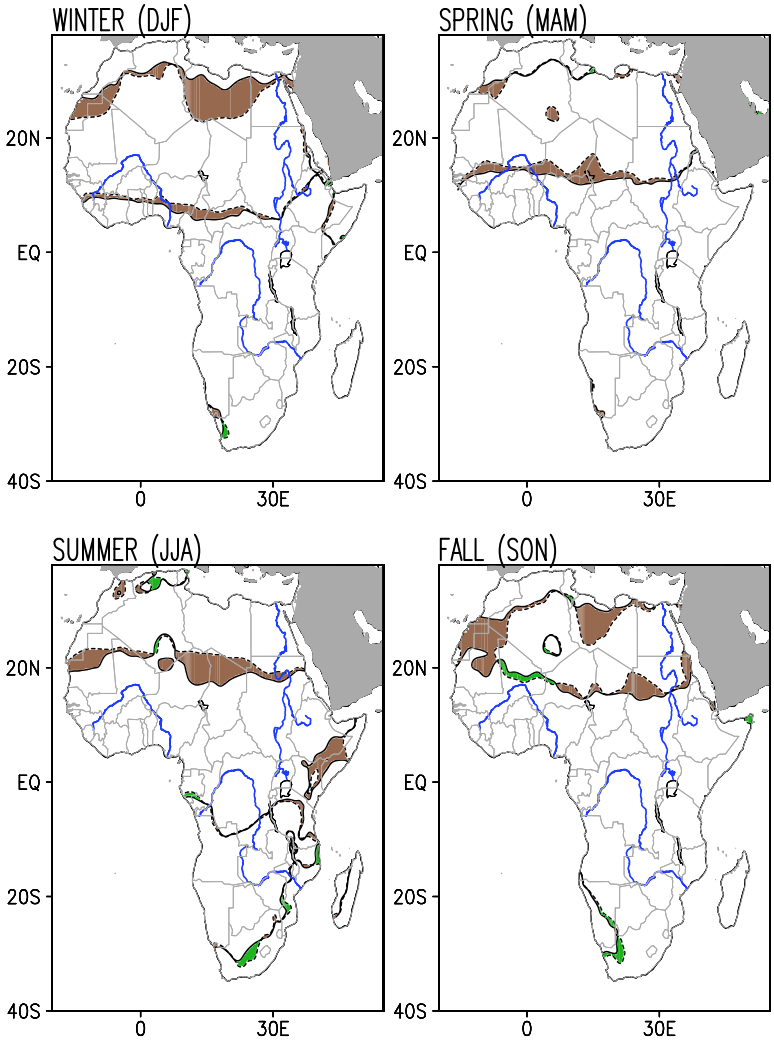

Figure 6. Advance or retreat of the Sahara Desert over the 1902–2013 period, seasonally. The dashed (solid) brown lines denote the 0.274mm day^{-1} precipitation isolines in the synthetic 1902 (2013) precipitation map obtained from the endpoint analysis. The brown (green) shaded areas denote desert advance (retreat).

The annual-mean desert advance (see Figure 7), provides context for the seasonal analysis and comports with the canonical desert definitions based on the annual-mean

rainfall threshold (Tucker and Nicholson 1999). The annual-mean advance shows primarily southward creep relative to the annual-mean desert boundaries (see Figure 5).

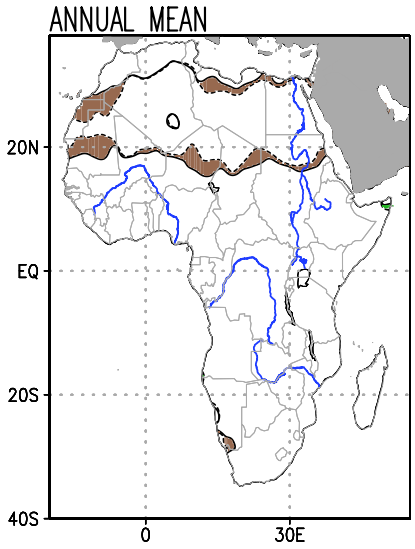

Figure 7. As in Figure 6, but for the advance or retreat of the Sahara Desert over the 1920–2013 period, annually. Desert identification here is fully consistent with the canonical desert definition based on annual-mean rainfall: a 100mmyr^{-1} threshold is used.

A quantitative analysis of the centennial change in the Sahara Desert's seasonal expanse is reported in Table 1. The primary analysis is based on the area-trend method but the endpoint method (Figures 6 and 7) is also used with both desert definitions to assess the sensitivity to analysis methods. The expansion has been largest (area-wise) in boreal winter (2,246,000 km^2, a 16% increase) and smallest in summer (876,000 km^2, an 11% increase) using the area-trend method. Estimates of desert expansion from the endpoint methods, yield maximum desert expansion in winter (2,348,000km^2, an 18% increase) and a minimum in spring (1,132,000km^2, an 11% increase). The endpoint method, however, yields significantly larger expansions in boreal summer and fall. As noted in Chapter 2, the two estimates can differ when multidecadal variability is potentially aliased into centennial trends—the case in summer and fall when the 65–70-yr

time scale AMO variability (Kavvada et al. 2013; Schlesinger and Ramankutty 1994) exerts strong influence on Sahel rainfall (Nigam and Ruiz-Barradas 2016; Zhang and Delworth 2006). Percent-wise, the desert expansion is largest in boreal fall.

	Thres-Hold (mm year^{-1})	**Winter (DJF)**	**Spring (MAM)**	**Summer (JJA)**	**Fall (SON)**
Climatological Sahara Extent (km^2)	**100**	13,686,000 (12,868,000)	10,540,000 (9,979,000)	7,725,000 (6,198,000)	7,583,000 (6,163,000)
	150	14,557,000 (13,872,000)	11,420,000 (10,782,000)	8,492,000 (7,351,000)	8,736,000 (8,018,000)
Sahara Expansion (km^2)	**100**	2,246,000 (2,348,000)	1,287,000 (1,132,000)	876,000 (1,594,000)	1,354,000 (2,048,000)
	150	1,800,000 (1,433,000)	1,009,000 (627,000)	847,000 (1,478,000)	999,000 (1,366,000)
Sahara Expansion (% of Climatological Area)	**100**	16% (18%)	12% (11%)	11% (26%)	18% (33%)
	150	12% (10%)	9% (6%)	10% (20%)	11% (17%)

Countries Affected (obtainable only from the endpoint method; the ones in bold are most impacted)		**Libya**, Egypt, Tunisia, Algeria, Morocco, **Western Sahara**, Mauritania, **Central African Rep.**, **Cameroon**, Nigeria, Guinea, Cote D'ivoire, Ghana, Togo, Benin	Morocco, Sudan, **Chad**, **Niger**, Nigeria, Burkina Faso, **Mali**, Senegal, Guinea	**Mauritania**, Western Sahara, Mali, Algeria, **Niger**, **Chad**, Libya, Sudan	**Libya**, Egypt, Algeria, Morocco, **Western Sahara**, **Mauritania**, Niger, Chad, **Sudan**

Table 1. Expansion of the Sahara Desert seasonally during 1902–2013, based on the movement of the 100 and 150mm yr^{-1} precipitation isolines. The expansion is computed using both area-trend and endpoint methods; endpoint values are in parentheses. The areal values are rounded off to the nearest 1000 km^2 (which is about 1/3 of the 0.5° grid cell area at the equator).

The sensitivity of the desert expansion rate to the desert-defining precipitation-threshold is also reported in Table 1. A less stringent definition, based on a 150mm yr^{-1} threshold, leads to more expansive deserts, not surprisingly, but also to smaller centennial expansions, indicating a tightening of the meridional precipitation gradient over the century. As Table 1 shows, with the less stringest threshold, percentages drop on both counts but the Sahara's expansion remains robust with the largest expansion, as before, in boreal winter (1,800,000 km^2, a 12% increase); this winter expansion, from the area-trend method, is largest both area- and percent-wise. The weakest expansion again is in summer (847,000 km^2, a 10% increase). Results from the endpoint method using the larger threshold are qualitatively similar to those obtained with the lower one.

The sensitivity analysis indicates that while desert expansion and the related area percentage vary somewhat with the desert definition and analysis method, one can reasonably conclude that the Sahara Desert has grown larger, area-wise, more in winter

than in summer; percentage-wise, the summer expansion can be larger in view of the smaller (nearly halved) climatological desert expanse in summer. The countries bearing the brunt of the Sahara's northwestward–northward advance in fall–winter are Libya, Mauritania, and Western Sahara; the southern advance principally impacts Niger, Chad, and Mauritania in summer, and Sudan in fall. One would be remiss to not note the summer desertification in the Horn of Africa, especially Ethiopia and Somalia. Notable against this backdrop of widespread desert advance (brown shading) over the northern continent is a sliver of green over Mali in fall, reflecting the Sahara's retreat.

The expansion of the Sahara Desert is also analyzed using the conventional annual-rainfall based desert definition. Table 2 notes the findings from the area-trend and endpoint methods for both the 100 and 150 mm yr^{-1} annual-rainfall thresholds. A slightly shorter period, beginning in 1920, is analyzed in the annual case in order to focus on the relatively stable rain gauge network period (S. Nicholson 2018, personal communication). During 1920–2013, the Sahara expanded by over 700,000km2 (or ~7,600km^2 yr^{-1}) based on the 100 mm yr^{-1} definition, indicating a ~10% expansion over its climatological area (7,426,000 km^2). The desert's southward creep (Figure 5) is the major contributor (~554 000 km^2 or 7.5%) to the expansion; the northward advance (182,000 km^2) contributes the remaining 2.5%. The linear trend in the Sahara Desert's expanse is sensitive to the analysis period from the potential aliasing of multidecadal variability, as noted earlier.

Unlike northern Africa, the southern continent is devoid of any desert advance, in any direction or season. To the contrary, the Namib/Kalahari Desert is found retreating,

albeit modestly, in austral winter (JJA) and spring (SON) when it is, climatologically, most expansive (cf. Figure 1).

Climatological Sahara extent (km^2)	**100 mm $year^{-1}$**	7,426,000 (6,890,000)
	150 mm $year^{-1}$	8,528,000 (7,947,000)
Sahara Expansion (km^2)	**100 mm $year^{-1}$**	711,000 (738,000)
	150 mm $year^{-1}$	718,000 (549,000)
Sahara Expansion (% of Climatological area)	**100 mm $year^{-1}$**	10% (11%)
	150 mm $year^{-1}$	8% (7%)
Countries Affected		Libya, Egypt, Algeria, **Western Sahara**, **Mauritania**, **Mali**, Niger, **Chad**, **Sudan**

Table 2. Expansion of the Sahara Desert annually during 1920-2013, based on the movement of the 100 and 150 mm yr-1 precipitation isolines. All other formatting as in Table 1.

3.4 The Sahara's expanse: variation and potential mechanisms

The Sahara Desert's expanse during the 1902–2013 period, and not just at its endpoints, is the focus of this section. The desert expanse in winter and summer is plotted in Figure 8, along with select indices of circulation and SST variability that can provide insights on causal mechanisms.

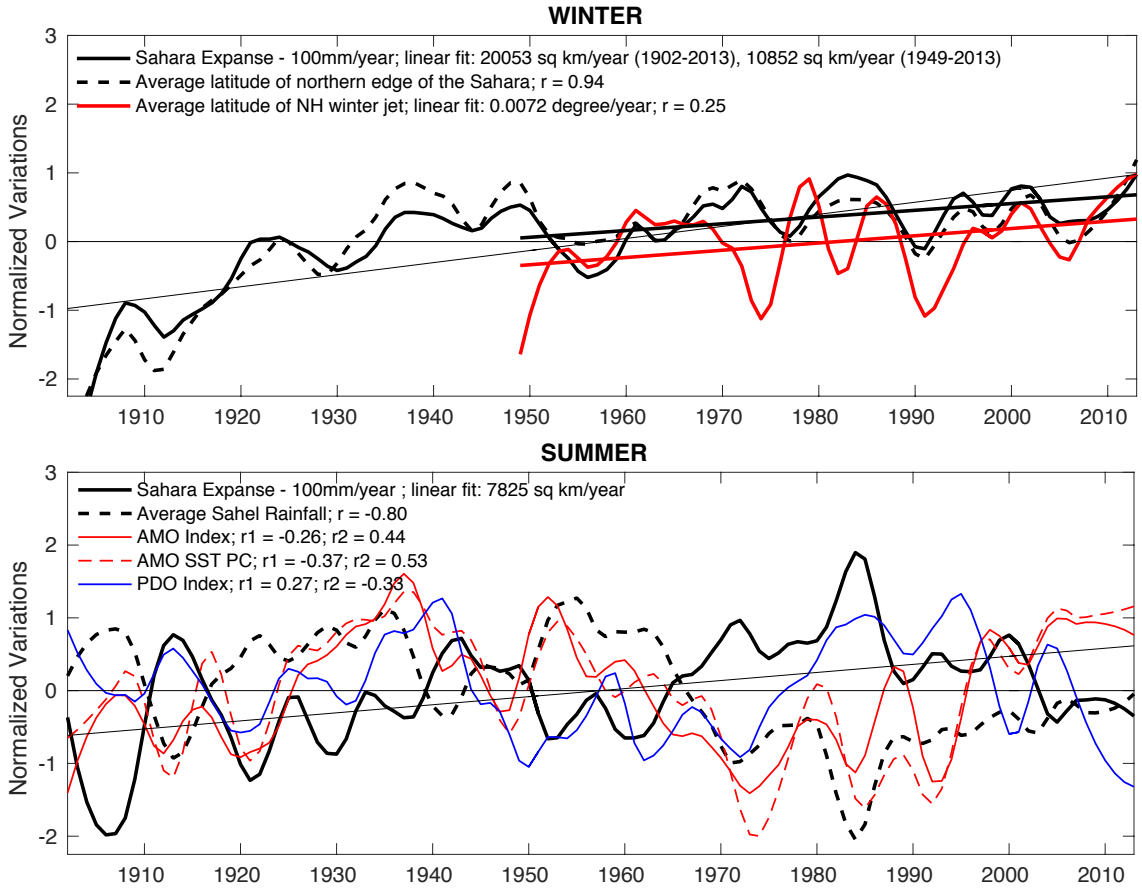

Figure 8. The Sahara Desert's expanse during 1902–2013. The boreal (top) winter and (bottom) summer expanse is shown using the thick solid black line. The thin black straight line is the linear fit to the desert expanse over the entire period; it is the basis of the area-trend analysis reported in Table 1. The thick black line is the linear fit to the winter desert expanse during 1949–2013—the period for which the latitude of the winter subtropical jet is plotted (solid red line, top). The Sahara expanse trend is significant at the 95% level in winter (both periods) and summer. Indices of SST and rainfall variability with potential links to the Sahara Desert's summer expanse are shown in (bottom), along with their correlation coefficients. For each index, r1 (r2) is the correlation between the index and Sahara expanse (Sahel rainfall). The AMO and PDO are displayed using their common SST indices; an SST principal component (PC)-based AMO index is also shown. The rainfall over the Sahel is plotted as well. All time series depict normalized anomalies after 10% Loess smoothing; the time series for the latitude of the Northern Hemisphere (NH) subtropical jet was smoothed with a 20% Loess function. All time series are normalized by their standard deviations.

The Sahara's winter expanse (Figure 8, top) is plotted together with the average latitude of the desert's northern edge using methods described in Chapter 2. The location

of the northern edge is of interest because the endpoint analysis (Figure 6) showed the twentieth-century expansion to be, principally, through the northern boundary. Not surprisingly, winter variations in the Sahara Desert expanse correlate well with the latitudinal position of the desert's northern boundary (Figure 8, top); r =0.94 (0.88) for smoothed (unsmoothed) indices; note that the high, statistically significant correlation emerges not just from similar upward trends but also from the correspondence in decadal variations. The linear fit to the Sahara's winter expanse is shown by the thin black line, which is the basis for the area-trend analysis (Table 1).

We hypothesize that the Sahara Desert's northward expansion in winter is due, largely, to the widening of the tropics (Seidel et al. 2008), based on canonical understanding of the desert's location relative to the descending branch of the Hadley circulation. As the descending branch terminus, which defines the width of the tropics, dynamically, is collocated with the core latitude of the subtropical jet in the upper troposphere, the latter serves as a convenient proxy for the width of the tropics. Previous studies have shown that the core of the northern winter subtropical jet has moved poleward in recent decades (Archer and Caldeira 2008). The 30°W–60°E sector-averaged latitudinal position of the jet in the NCEP-NCAR reanalysis (Kalnay et al. 1996), computed using these authors' method, is shown by the red line in Figure 8 (top), along with a linear fit to its variation. While both the Sahara's expanse and the subtropical jet-latitude depict upward trends—and nearly identical ones (0.98% and 1.05% yr^{-1}, respectively) when for the same period (1949–2013)—the two variations are modestly correlated (r=0.25; not significant at the 95% level), notwithstanding periods (1950–65 and 1985–2013) when they track each other closely. The similar upward trends over the

recent 65-yr period lend credence to the hypothesis linking the Sahara's increasing winter expanse (and northern extent) to a secular change in the width of the tropics. The modest correlation between the two on decadal (and shorter) time scales, while detracting, attests to the influence of other processes on the desert expanse in winter, such as tropical SSTs and the North Atlantic Oscillation (through its impact on winter storm tracks; e.g., (Linkin and Nigam 2008)).

Summer variations in the Sahara Desert's expanse, unlike winter ones, arise mainly from the north–south movements of its southern boundary, which borders the Sahel. The summer expanse (solid black line) exhibits both an upward trend, highlighted by the linear fit (thin black straight line), and notable decadal–multidecadal variations. As areal changes result from the equatorward advance or poleward retreat of the desert's southern edge, the Sahara's summer expanse should be inversely linked to Sahel rainfall (defined in section 2.1), which is plotted with a dashed black line. The inverse relationship can be visually discerned: for example, the drying of the Sahel (a multidecadal decline in Sahel rainfall from the mid-1950s to the mid-1980s) is coincident with the Sahara's expansion; the full-period correlation ($r=-0.80$; significant at the 95% level) points to a strong inverse relationship. The anticorrelation allows tapping into extensive analyses of Sahel rainfall variability in the attribution of the summer waxing and waning of the Sahara Desert.

The Sahel rainfall has been linked to AMO variability among other processes. To assess links between AMO and the Sahara's extent, two markers of AMO variability are plotted in Figure 8 (bottom) along with their correlations to the Sahara's expanse and Sahel rainfall. The AMO SST principal component (dashed red line), obtained from an

evolution-centric spatiotemporal analysis of seasonal SST anomalies in the twentieth century (Guan and Nigam 2009), shows higher correlations with both the Sahara's expanse (r=-0.37; significant at the 80% level) and Sahel rainfall (r=0.53; significant at the 95% level) in boreal summer.

Decadal SST variability in the Pacific basin, as typified by the Pacific decadal oscillation (Mantua et al. 1997), is also linked with Sahel rainfall (Nigam and Ruiz-Barradas 2016; Villamayor and Mohino 2015) albeit not as strongly as the AMO. The PDO index, shown in Figure 8 (solid blue line), is correlated with Sahel rainfall and the Sahara's expanse at -0.33 (significant at the 90% level) and 0.27 (significant at the 75% level), respectively. A statistical link between the PDO and Sahel rainfall seems more intriguing than the rainfall's link with the AMO because the AMO SST anomalies are proximal, with their tropical footprints offering potential mechanisms for their influence. In contrast, the PDO SST anomalies are distant and focused in the midlatitudes, disadvantaging them from the influence potential, especially as only the tropical SST anomalies are generally viewed as influential on faraway regions. Interestingly, these disadvantages disappear once one recognizes that the PDO is not without tropical links Guan and Nigam (2008) showed the PDO counterpart in their spatiotemporal analysis [called by them Pacific decadal variability–North Pacific (PDV-NP)] to be linked with the tropical Indian and Pacific basin SSTs; see also Deser et al. (2004). The PDO's modest influence on Sahel rainfall, if realized through its tropical Indian Ocean footprints, would be consistent with the findings of Hagos and Cook (2008).

Secular change is often characterized using the century-long linear trends in observational records, as for the Sahara's expanse in Figure 8. The linear trend is

however susceptible to the aliasing of multidecadal variability should the latter be prominently manifest in the record, as is the case in summer (cf. Figure 8).

The origin of the 112-yr linear trend (referred to as the secular trend) in the Sahara's summer expanse remains to be elucidated; the elucidation is challenging, especially, for an observational analysis. Trends on centennial and longer time scales can potentially result from the interaction of multidecadal variabilities (e.g., the PDO and AMO) and, of course, from the increasing concentration of greenhouse gases and aerosol loading (Held et al. 2006) and the related change in SST distribution (Nigam and Ruiz-Barradas 2016).

The seasonally stratified analysis of hydroclimate trends—the focus of the study—was complemented by analyses of the annual-mean trends. The latter, more directly relatable to deserts in view of the canonical annual rainfall-based desert definition, also revealed impressive expansion rates for the Sahara Desert over the twentieth century (Table 1). The rate is however sensitive to the analysis period, from exposure to the aliasing of multidecadal variability (e.g., AMO and PDO) and variability of the rain gauge network. Figure 9 plots the linear expansion rate of the Sahara Desert's annual expanse over two different multidecadal periods, both ending in 2013; the rates are quite variable, ranging from 9.9% to 23%, likely from the impact of the coarse rain gauge network in the early part of the 20th century.

The aliasing of multidecadal variability in the linear trend in the Sahara's annual-mean expanse is directly investigated during the relatively stable rain-gauge network period (1920 onwards) in Figure 9. The AMO and PDO influences are removed from the precipitation record via linear regression. The seasonally stratified precipitation fields are regressed onto the seasonal AMO and PDV-NP SST principal components (PCs, which

are orthonormal; (Nigam et al. 2011)) over the full period (1902–2013). The influence of these multidecadal variability modes is computed by multiplying their time-independent regression coefficients by their time-varying PC, seasonally. The influence is then subtracted from the precipitation record, and the desert expanse recomputed, as before.

The annual-mean Sahara Desert expanse sans the multidecadal modes' influence is shown in Figure 9 by the red curve. The AMO's and PDO's influence is strong during the 1970s–90s when the red curve diverges from the black one; their contribution to the drying of the Sahel during the 1950s–80s is evident. The different linear trends of the two time series indicate that about two-thirds of the; 10% increase in the Sahara Desert's annual-mean expanse during 1920-2013 is attributable to multidecadal SST variability, and the remaining one-third to the rising greenhouse gas concentrations and aerosol loadings, and other factors.

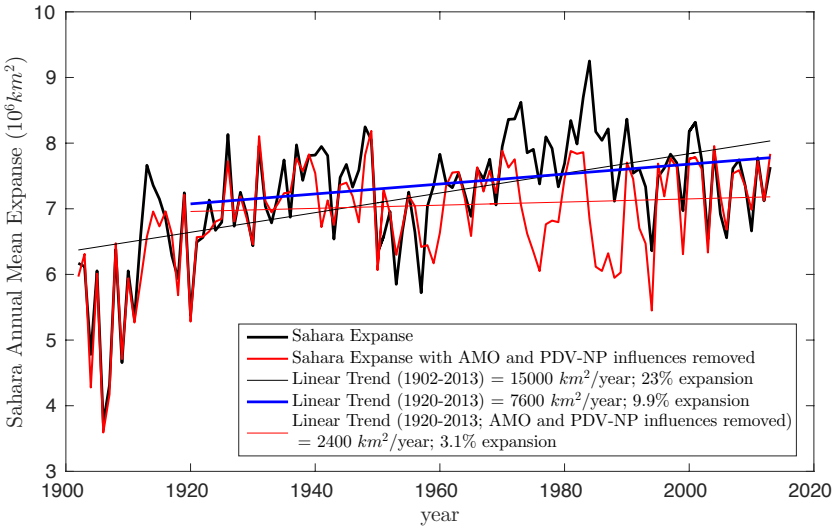

Figure 9. Annual-mean Sahara Desert expanse (km^2; computed from the area-trend method). Linear trends are shown for 1902–2013 (thin black line) and 1920–2013 (thick blue line); the values are noted in the legend. The red curve and the corresponding 1920–2013 linear trend (thin red line) track desert expanse after removal of the AMO's and PDO's influence from the precipitation data set. The area-expansion percentages are all computed using the 1902–2013 climatological desert expanse.

Chapter 4. Summary and conclusions

The footprints of climate change over the African continent are widely noted (Niang et al. 2014) but even region-specific descriptions seldom stray from the annual-mean displays of hydroclimate trends—and this over the African continent, where the seasonal waxing and waning of the Sahara Desert and the complementary retraction and expansion of Sahel rainfall rule the northern continent. Southern Hemisphere Africa is also no stranger to the munificence of the seasonal cycle, which brings rainfall and life to vast stretches of the Namib–Kalahari Desert in austral summer. The utility of the seasonal perspective in climate change (i.e., seasonally stratified centennial trends in precipitation and near-surface air temperature) for long-term water resource management cannot, of course, be overstated.

The centennial SAT trends are larger over the northern continent, especially in the northwestern sector and North Africa (Algeria and Libya) where they are often greater than 1.6°C century^{-1}. The trends are furthermore pronounced in boreal summer, amplifying the regional seasonal cycle (i.e., making hot summers even hotter and exacerbating heat-related distress). Another focal point of large SAT trends over north Africa is the region to the west of the White Nile (central-southern Sudan). For context, these SAT trends are not much smaller than the largest SAT trends over North America (e.g., (Nigam et al. 2017)) that are manifest over western-central Canada in winter. Centennial precipitation trends, especially the drying ones, are notable over the tropical continent (i.e., in the region between the Sahara and the Namib–Kalahari deserts). River-basin-wise, impressive drying trends are found in the source region of the Niger River from spring to fall (i.e., in the local rainy seasons); the decline is impressive because it

represents a 10%-25% decline in seasonal rainfall over the course of the twentieth century. Another focal point of declining rainfall is the Congo River basin, and the Blue Nile source region around Lake Tana in Ethiopia (the latter in boreal summer, the peak rainfall season).

When viewed together, the key features of the centennial drying trends can be interpreted as the southward expansion of the Sahara Desert during boreal spring to fall, or alternatively, as the equatorward retreat of the northern edge of the Sahel rainfall belt. The winter rainfall decline in northern Africa, likewise, alludes to the Sahara's northward advance. We show that the Sahara Desert has expanded significantly over the twentieth century—by 11%–18% depending on the season—using conservative estimates from the area-trend method. In winter, the desert's northward advance arises from the secular expansion of the tropics and the resulting subtropical descent (and desertification). The southward expansion in summer is linked to the SST variability in the Atlantic and Pacific basins on multidecadal time scales, through the Atlantic multidecadal oscillation's (AMO) and Pacific decadal oscillation's (PDO) impact on Sahel rainfall. On centennial time scales, the summer expansion is related to aliased multidecadal variabilities and the increasing concentration of greenhouse gases and aerosol loading (Held et al. 2006). There are other interesting features such as the increasing rainfall trends over the African Great Lakes during austral spring and summer. Are these generated from trends in regional circulation and related moisture transports (and convergence) and/or from trends in the seasonal cross-equatorial transition/position of the intertropical convergence zone (ITCZ)? The positive (negative) rainfall trends over southern (northern) equatorial

Africa, including the African Great Lakes, are not inconsistent with the latter possibility. Regardless, these questions merit further analysis.

A follow-on analysis to investigate the mechanisms generating the seasonality and regionality of the hydroclimate trends is clearly needed to advance the process-level understanding of the origin of these trends. The challenge is patent as observational records, especially of near-surface (e.g., 925-hPa) winds, evapotranspiration, and soil moisture are sparse over the African continent while the current IPCC-class climate system models are unable to simulate the hydroclimate trends in historical simulations, precluding the use of models in attribution analysis.

References

Archer, C. L., and K. Caldeira, 2008: Historical trends in the jet streams. *Geophysical Research Letters*, **35,** 6.

Becker, A., P. Finger, A. Meyer-Christoffer, B. Rudolf, K. Schamm, U. Schneider, and M. Ziese, 2013: A description of the global land-surface precipitation data products of the Global Precipitation Climatology Centre with sample applications including centennial (trend) analysis from 1901-present. *Earth System Science Data*, **5,** 71-99.

Biasutti, M., 2013: Forced Sahel rainfall trends in the CMIP5 archive. *Journal of Geophysical Research-Atmospheres*, **118,** 1613-1623.

Biasutti, M., and A. Giannini, 2006: Robust Sahel drying in response to late 20th century forcings. *Geophysical Research Letters*, **33,** 4.

Breman, H., and C. T. Dewit, 1983: RANGELAND PRODUCTIVITY AND EXPLOITATION IN THE SAHEL. *Science*, **221,** 1341-1347.

Busby, J. W., K. H. Cook, E. K. Vizy, T. G. Smith, and M. Bekalo, 2014: Identifying hot spots of security vulnerability associated with climate change in Africa. *Climatic Change*, **124,** 717-731.

Charney, J., 1975: Dynamics of deserts and drought in the Sahel. *Quarterly Journal of the Royal Meteorological Society*, **101,** 193-202.

Chou, C., J. C. H. Chiang, C. W. Lan, C. H. Chung, Y. C. Liao, and C. J. Lee, 2013: Increase in the range between wet and dry season precipitation. *Nature Geoscience*, **6,** 263-267.

Collins, J. M., 2011: Temperature Variability over Africa. *Journal of Climate*, **24,** 3649-

3666.

Cook, K. H., and E. K. Vizy, 2015: Detection and Analysis of an Amplified Warming of the Sahara Desert. *Journal of Climate*, **28,** 6560-6580.

Dai, A., and K. Trenberth, 2003: New Estimates of Continental Discharge and Oceanic Freshwater Transport. *Proceedings of the Symposium on Observing and Understanding the Variability of Water in Weather and Climate, 83rd Annual AMS Meeting*, 1-18.

Deser, C., A. S. Phillips, and J. W. Hurrell, 2004: Pacific interdecadal climate variability: Linkages between the tropics and the North Pacific during boreal winter since 1900. *Journal of Climate*, **17,** 3109-3124.

Dong, B. W., and R. Sutton, 2015: Dominant role of greenhouse-gas forcing in the recovery of Sahel rainfall. *Nature Climate Change*, **5,** 757-U173.

Ebisuzaki, W., 1997: A method to estimate the statistical significance of a correlation when the data are serially correlated. *Journal of Climate*, **10,** 2147-2153.

Enfield, D. B., A. M. Mestas-Nunez, and P. J. Trimble, 2001: The Atlantic multidecadal oscillation and its relation to rainfall and river flows in the continental US. *Geophysical Research Letters*, **28,** 2077-2080.

Evan, A. T., C. Flamant, M. Gaetani, and F. Guichard, 2016: The past, present and future of African dust. *Nature*, **531,** 493-+.

Feng, X., A. Porporato, and I. Rodriguez-Iturbe, 2013: Changes in rainfall seasonality in the tropics. *Nature Climate Change*, **3,** 811-815.

Fields, S., 2005: Spheres of influence - Continental divide - Why Africa's climate change burden is greater. *Environmental Health Perspectives*, **113,** A534-A537.

Folland, C. K., T. N. Palmer, and D. E. Parker, 1986: SAHEL RAINFALL AND WORLDWIDE SEA TEMPERATURES, 1901-85. *Nature*, **320,** 602-607.

Giannini, A., R. Saravanan, and P. Chang, 2003: Oceanic forcing of Sahel rainfall on interannual to interdecadal time scales. *Science*, **302,** 1027-1030.

Guan, B., and S. Nigam, 2008: Pacific sea surface temperatures in the twentieth century: An evolution-centric analysis of variability and trend. *Journal of Climate*, **21,** 2790-2809.

——, 2009: Analysis of Atlantic SST Variability Factoring Interbasin Links and the Secular Trend: Clarified Structure of the Atlantic Multidecadal Oscillation. *Journal of Climate*, **22,** 4228-4240.

Hagos, S. M., and K. H. Cook, 2008: Ocean warming and late-twientieth-century Sahel drought and recovery. *Journal of Climate*, **21,** 3797-3814.

Hansen, J., R. Ruedy, M. Sato, and K. Lo, 2010: GLOBAL SURFACE TEMPERATURE CHANGE. *Reviews of Geophysics*, **48,** 29.

Harris, I., P. D. Jones, T. J. Osborn, and D. H. Lister, 2014: Updated high-resolution grids of monthly climatic observations - the CRU TS3.10 Dataset. *International Journal of Climatology*, **34,** 623-642.

Held, I. M., T. L. Delworth, J. Lu, K. L. Findell, and T. R. Knutson, 2006: Simulation of Sahel drought in the 20th and 21st centuries (vol 102, pg 17891, 2005). *Proceedings of the National Academy of Sciences of the United States of America*, **103,** 1152-1153.

Hoerling, M., J. Hurrell, J. Eischeid, and A. Phillips, 2006: Detection and attribution of

twentieth-century northern and southern African rainfall change. *Journal of Climate*, **19,** 3989-4008.

Hulme, M., R. Doherty, T. Ngara, M. New, and D. Lister, 2001: African climate change: 1900-2100. *Climate Research*, **17,** 145-168.

James, R., and Coauthors, 2018: EVALUATING CLIMATE MODELS WITH AN AFRICAN LENS. *Bulletin of the American Meteorological Society*, **99,** 313-336.

Kalnay, E., and Coauthors, 1996: The NCEP/NCAR 40-year reanalysis project. *Bulletin of the American Meteorological Society*, **77,** 437-471.

Kavvada, A., A. Ruiz-Barradas, and S. Nigam, 2013: AMO's structure and climate footprint in observations and IPCC AR5 climate simulations. *Climate Dynamics*, **41,** 1345-1364.

Knight, J. R., C. K. Folland, and A. A. Scaife, 2006: Climate impacts of the Atlantic Multidecadal Oscillation. *Geophysical Research Letters*, **33,** 4.

Linkin, M. E., and S. Nigam, 2008: The north pacific oscillation-west Pacific teleconnection pattern: Mature-phase structure and winter impacts. *Journal of Climate*, **21,** 1979-1997.

Maidment, R. I., R. P. Allan, and E. Black, 2015: Recent observed and simulated changes in precipitation over Africa. *Geophysical Research Letters*, **42,** 8155-8164.

Mantua, N. J., S. R. Hare, Y. Zhang, J. M. Wallace, and R. C. Francis, 1997: A Pacific interdecadal climate oscillation with impacts on salmon production. *Bulletin of the American Meteorological Society*, **78,** 1069-1079.

Martin, E. R., and C. D. Thorncroft, 2014: The impact of the AMO on the West African

monsoon annual cycle. *Quarterly Journal of the Royal Meteorological Society*, **140,** 31-46.

Mohino, E., S. Janicot, and J. Bader, 2011: Sahel rainfall and decadal to multi-decadal sea surface temperature variability. *Climate Dynamics*, **37,** 419-440.

Niang, I., and Coauthors, 2014: Africa. *Climate Change 2014: Impacts, Adaptation, and Vulnerability, Pt B: Regional Aspects: Working Group Ii Contribution to the Fifth Assessment Report of the Intergovernmental Panel on Climate Change*, V. R. Barros, and Coauthors, Eds., Cambridge Univ Press, 1199-1265.

Nicholson, S., 2000: Land surface processes and Sahel climate. *Reviews of Geophysics*, **38,** 117-139.

Nicholson, S. E., 2001: Climatic and environmental change in Africa during the last two centuries. *Climate Research*, **17,** 123-144.

Nicholson, S. E., and E. Kim, 1997: The relationship of the El Nino Southern oscillation to African rainfall. *International Journal of Climatology*, **17,** 117-135.

Nigam, S., and S. C. Chan, 2009: On the Summertime Strengthening of the Northern Hemisphere Pacific Sea Level Pressure Anticyclone. *Journal of Climate*, **22,** 1174-1192.

Nigam, S., and A. Ruiz-Barradas, 2016: Key role of the Atlantic multidecadal oscillation in twentieth century drought and wet periods over the US Great Plains and the Sahel. *Dynamics and Predictability of Large-Scale, High-Impact Weather and Climate Events*, J. Li, R. Swinbank, H. Volkert, and R. Grotjahn, Eds., Cambridge University Press, 255-270.

Nigam, S., B. Guan, and A. Ruiz-Barradas, 2011: Key role of the Atlantic Multidecadal

Oscillation in 20th century drought and wet periods over the Great Plains. *Geophysical Research Letters*, **38,** 6.

Nigam, S., N. P. Thomas, A. Ruiz-Barradas, and S. J. Weaver, 2017: Striking Seasonality in the Secular Warming of the Northern Continents: Structure and Mechanisms. *Journal of Climate*, **30,** 6521-6541.

Omondi, P., L. A. Ogallo, R. Anyah, J. M. Muthama, and J. Ininda, 2013: Linkages between global sea surface temperatures and decadal rainfall variability over Eastern Africa region. *International Journal of Climatology*, **33,** 2082-2104.

Rayner, N. A., and Coauthors, 2003: Global analyses of sea surface temperature, sea ice, and night marine air temperature since the late nineteenth century. *Journal of Geophysical Research-Atmospheres*, **108,** 37.

Rohde, R., and Coauthors, 2013: A New Estimate of the Average Earth Surface Land Temperature Spanning 1753 to 2011. *Geoinformatics & Geostatistics: An Overview*, **1,** 1 7.

Rowell, D. P., B. B. B. Booth, S. E. Nicholson, and P. Good, 2015: Reconciling Past and Future Rainfall Trends over East Africa. *Journal of Climate*, **28,** 9768-9788.

Santer, B. D., and Coauthors, 2000: Statistical significance of trends and trend differences in layer-average atmospheric temperature time series. *Journal of Geophysical Research-Atmospheres*, **105,** 7337-7356.

Schlesinger, M. E., and N. Ramankutty, 1994: AN OSCILLATION IN THE GLOBAL CLIMATE SYSTEM OF PERIOD 65-70 YEARS. *Nature*, **367,** 723-726.

Schneider, U., A. Becker, P. Finger, A. Meyer-Christoffer, M. Ziese, and B. Rudolf,

2014: GPCC's new land surface precipitation climatology based on quality-controlled in situ data and its role in quantifying the global water cycle. *Theoretical and Applied Climatology*, **115,** 15-40.

Schreck, C. J., and F. H. M. Semazzi, 2004: Variability of the recent climate of eastern Africa. *International Journal of Climatology*, **24,** 681-701.

Seidel, D. J., Q. Fu, W. J. Randel, and T. J. Reichler, 2008: Widening of the tropical belt in a changing climate. *Nature Geoscience*, **1,** 21-24.

Tucker, C. J., and S. E. Nicholson, 1999: Variations in the size of the Sahara Desert from 1980 to 1997. *Ambio*, **28,** 587-591.

Tucker, C. J., H. E. Dregne, and W. W. Newcomb, 1991: EXPANSION AND CONTRACTION OF THE SAHARA DESERT FROM 1980 TO 1990. *Science*, **253,** 299-301.

Villamayor, J., and E. Mohino, 2015: Robust Sahel drought due to the Interdecadal Pacific Oscillation in CMIP5 simulations. *Geophysical Research Letters*, **42,** 1214-1222.

Vizy, E. K., and K. H. Cook, 2017: Seasonality of the Observed Amplified Sahara Warming Trend and Implications for Sahel Rainfall. *Journal of Climate*, **30,** 3073-3094.

Weare, B. C., and J. S. Nasstrom, 1982: EXAMPLES OF EXTENDED EMPIRICAL ORTHOGONAL FUNCTION ANALYSES. *Monthly Weather Review*, **110,** 481-485.

Williams, A. P., and C. Funk, 2011: A westward extension of the warm pool leads to a

westward extension of the Walker circulation, drying eastern Africa. *Climate Dynamics*, **37,** 2417-2435.

Zhang, R., and T. L. Delworth, 2006: Impact of Atlantic multidecadal oscillations on India/Sahel rainfall and Atlantic hurricanes. *Geophysical Research Letters*, **33,** 5.

Zhang, Y., J. M. Wallace, and D. S. Battisti, 1997: ENSO-like interdecadal variability: 1900-93. *Journal of Climate*, **10,** 1004-1020.

Zhou, L. M., 2016: Desert Amplification in a Warming Climate. *Scientific Reports*, **6,** 13.